

Reexamining doped two-legged Hubbard ladders

Yang Shen¹,²,³ Guang-Ming Zhang,^{2,3} and Mingpu Qin^{1,4,*}

¹Key Laboratory of Artificial Structures and Quantum Control (Ministry of Education), School of Physics and Astronomy, Shanghai Jiao Tong University, Shanghai 200240, China

²State Key Laboratory of Low-Dimensional Quantum Physics and Department of Physics, Tsinghua University, Beijing 100084, China

³Frontier Science Center for Quantum Information, Beijing 100084, China

⁴Hefei National Laboratory, Hefei 230088, China



(Received 26 April 2023; revised 16 September 2023; accepted 18 September 2023; published 11 October 2023)

We revisit the ground state of the Hubbard model on two-legged ladders in this paper. We perform density matrix renormalization group (DMRG) calculations on large system sizes with large numbers of kept states and perform extrapolation of DMRG results with truncation errors in the converged region. We find that the superconducting correlation exponent K_{sc} extracted from the pair-pair correlation is very sensitive to the position of the reference bond, reflecting a huge boundary effect on it. By systematically removing the effects from boundary conditions, finite sizes, and truncation errors in DMRG, we obtain more accurate values of K_{sc} and K_ρ with DMRG. With these exponents, we confirm that the two-legged Hubbard model is in the Luther-Emery liquid phase with $K_{sc} \cdot K_\rho = 1$ from tiny doping near half filling to 1/8 hole doping. When the doping is increased to $\delta \gtrsim 1/6$, the behaviors of charge, pairing, and spin correlations do not change qualitatively, but the relationship $K_{sc} \cdot K_\rho = 1$ is likely to be violated. With the further increase of the doping to $\delta = 1/3$, the quasi-long-ranged charge correlation turns into a true long-ranged charge order, and the spin gap is closed, while the pair-pair correlation still decays algebraically. Our work provides a standard way to analyze the correlation functions when studying systems with open boundary conditions.

DOI: [10.1103/PhysRevB.108.165113](https://doi.org/10.1103/PhysRevB.108.165113)

I. INTRODUCTION

The Hubbard model [1–3] is the prototype lattice model of interacting fermions and plays a paradigmatic role in correlated electron physics [4]. The connection of the two-dimensional Hubbard model and the related t - J model to cuprate superconductors has been debated [5–14] ever since the discovery of the first cuprate superconductor [15]. Because there is no rigorous analytic solution to the Hubbard model beyond one dimension [16], most studies of it rely on numerical methods [17].

Quasi-one-dimensional systems, such as two-legged Hubbard ladders, have been extensively studied [18–23]. On the one hand, the correlations in the two-legged Hubbard model can be taken as the precursor to the possible superconducting and charge density wave (CDW) instabilities in two-dimensional systems. On the other hand, two-legged systems can be accurately solved using the density matrix renormalization group (DMRG) [24–26]. Early analytic and numerical works [18–20] demonstrate that slightly doped ladders can be categorized into the Luther-Emery liquid phase [27,28], which promises a single gapless charge mode and a gapped spin mode (labeled as C1S0 in the literature [19,29,30]).

The Luther-Emery liquid phase is characterized by the algebraic decay of both charge (with exponent K_ρ) and pair-pair

correlations (with exponent K_{sc}). Moreover, the exponents are related and satisfy the relationship $K_{sc} \cdot K_\rho = 1$ [27,29,30]. Numerically, whether the relationship $K_{sc} \cdot K_\rho = 1$ holds has been debated, with both affirmative [29] and negative [31,32] results. K_ρ can be usually extracted from the Friedel oscillations [33] in a system with open boundaries. The difficulty of obtaining a reliable K_{sc} lies in the subtlety in the extraction of the exponent K_{sc} from the pair-pair correlation function, which usually oscillates with distance under the influence of the modulation of charge density [29,31,32]. In the strong-coupling limit of the t - J model with hole doping $\delta \rightarrow 0$, bosonization calculation yields $K_{sc} = 1/2$ [34,35]. Previous DMRG calculations found the decay of the superconducting correlation function to be much faster than $1/K_\rho$ at small doping, hence violating the relationship $K_{sc} \cdot K_\rho = 1$ [31,32]. However, later results [29] found that the relationship of the exponents holds. Therefore it is natural to ask to what degree, e.g., doping levels, the relationship of the exponents holds in the two-legged Hubbard model.

In this paper, we revisit the ground state of the two-legged Hubbard model. We study dopings ranging from 1/16 to as large as 1/3, trying to figure out the boundary of the Luther-Emery liquid phase by examining the behaviors of charge, spin, and pair-pair correlations. We focus on the issue of whether the relationship $K_{sc} \cdot K_\rho = 1$ holds. We employ DMRG in this paper, which can provide extremely accurate results for ladder systems nowadays with the increase in computational power. We push the bond dimension to a value as large as 9500 (with truncation error of the order of 10^{-7}) to

*qinmingpu@sjtu.edu.cn

TABLE I. Summary of the extracted exponents and correlation lengths. K_ρ and K_{sc} are the exponents for the algebraic decay of charge density and pair-pair correlations. ξ_s and ξ_G are the correlation lengths for the spin correlation (local magnetization) and single-particle Green's function. Quantities not listed in the table are ill defined.

Hole doping	K_ρ	K_{sc}	ξ_s	ξ_G	$K_\rho \cdot K_{sc}$
1/16	1.28(3)	0.85(5)	22.26(7)	15.8(3)	1.09(9)
1/12	1.13(3)	0.95(3)	28.9(2)	18.4(5)	1.07(6)
1/8	1.02(4)	0.98(2)	45.3(3)	26.8(2)	1.00(6)
1/6	1.01(4)	1.13(3)	67.6(2)	36(2)	1.14(8)
1/4		1.05(6)	107(2)	50(2)	
1/3		1.10(8)			

achieve a high level of accuracy for the Hubbard model on ladders [29,31,32]. More importantly, we study large system sizes and make sure the extracted exponents are free from the finite-size effect. We also vary the position of the reference bond in the calculation of pair-pair correlation functions to get rid of the effect of open boundaries, which turn out to have a huge impact on the extracted exponent K_{sc} (the error caused by the open boundaries could be as large as 50%, as will be shown in the discussion of results). With this careful treatment of the effects of boundary conditions, finite sizes, and truncation error in DMRG calculations, we obtain more accurate values of K_ρ and K_{sc} with which we can resolve the previous controversy as to whether the relationship $K_{sc} \cdot K_\rho = 1$ holds and determine the precise phase boundary of the Luther-Emery liquid phase.

The main results are summarized in Table I. We focus on the strongly correlated region with $U/t = 8$. From tiny doping near half filling to $\delta = 1/8$, the two-legged Hubbard model is found to be in the Luther-Emery liquid phase with algebraic decay of pair-pair and charge correlations and exponential decay of the spin correlation. The exponents of charge and pairing correlations also satisfy the relationship $K_{sc} \cdot K_\rho = 1$. In this region, $K_{sc} < K_\rho$, which means that the superconducting correlation is the dominant correlation. The increase of the hole doping tends to suppress the pairing correlations and consequently enhances the charge correlation. When the doping is increased to 1/6, the characterization of charge, pairing, and spin correlations does not change qualitatively, but the exponents of the superconducting and charge correlations seem to violate the $K_{sc} \cdot K_\rho = 1$ relationship. The system also switches to a charge-correlation-dominant phase with $K_\rho < K_{sc}$. When the doping level is increased further, i.e., for $\delta = 1/4$ and $1/3$, K_ρ becomes ill defined, and the charge correlation is likely to be long ranged. The spin gap is closed at 1/3 doping, but the algebraic decay of pair-pair correlation functions remains.

We notice that the K_ρ values in Table I are consistent with recent results obtained from infinite-system matrix product states [36].

The remainder of this paper is organized as follows. In Sec. II we introduce the Hubbard model and discuss the calculation details. We then provide results for different doping levels in Sec. III. We show the long-distance behaviors of the pairing, charge, spin, and single-particle correlations.

We extract the exponents and correlation lengths from them by carefully analyzing the effects from boundary conditions, finite sizes, and truncation error in DMRG calculations. We finally summarize this work in Sec. IV.

II. MODEL AND METHODOLOGY

The Hamiltonian of the Hubbard model is

$$\hat{H} = - \sum_{(i,j),\sigma} t_{ij} (\hat{c}_{i\sigma}^\dagger \hat{c}_{j\sigma} + \text{H.c.}) + U \sum_i \hat{n}_{i\uparrow} \hat{n}_{i\downarrow}, \quad (1)$$

where $\hat{c}_{i\sigma}^\dagger$ ($\hat{c}_{j\sigma}$) creates (annihilates) an electron at site $i = (x_i, y_i)$ with spin σ and U represents the on-site Coulomb interaction. We only consider nearest hopping t and set $U = 8t$. $\hat{n}_i = \sum_\sigma \hat{c}_{i\sigma}^\dagger \hat{c}_{i\sigma}$ is the electron number operator.

We focus on ladders with width $L_y \equiv 2$ and length L_x ; so there are in total $N = L_x \times L_y$ lattice sites. The average hole concentration away from half filling is defined as $\delta = N_h/N$ with $N_h = \sum_i (1 - \langle \hat{n}_i \rangle)$. We apply a one-site pinning field [an additional term $h_m \cdot \hat{S}_{0z}$ with $h_m = 0.5$ is added to the Hamiltonian in Eq. (1)] at the left edge of the ladder, which allows us to detect the local magnetization $\langle \hat{S}_i^z \rangle [= 1/2 \times (\langle \hat{n}_{i\uparrow} \rangle - \langle \hat{n}_{i\downarrow} \rangle)]$ instead of the more demanding correlation functions. We also measure the d -wave pair-pair correlation function defined as $D(r) = \langle \hat{\Delta}_i^\dagger \hat{\Delta}_{i+r} \rangle$ with $\hat{\Delta}_i^\dagger = \hat{c}_{(i,1),\uparrow}^\dagger \hat{c}_{(i,2),\downarrow}^\dagger - \hat{c}_{(i,1),\downarrow}^\dagger \hat{c}_{(i,2),\uparrow}^\dagger$ creating a singlet on the rungs [29,37]. All other physical observables are defined at first mention.

We employ the DMRG method, which can provide extremely accurate results for ladder systems. We push the bond dimension in the DMRG calculations up to $m = 9500$ with typical truncation errors ϵ of the order of 10^{-7} . Extrapolations with truncation errors ϵ are also performed to remove the tiny residual truncation errors. We study systems as long as 192 sites to get rid of the finite-size effect. More importantly, when calculating the pair-pair correlation function, we vary the position of the reference bond to ensure that the effect of boundary conditions is absent. It turns out that the boundary conditions have a huge effect (could cause an error as large as 50%) on the extracted value of K_{sc} . With this careful treatment of the possible errors, we provide reliable results for the charge density, pair-pair correlations, and local magnetization.

III. RESULTS AND DISCUSSION

A. 1/8 doping level

We start with the 1/8 doping case, which draws dramatic interests because of the intertwined spin, charge, and pairing correlation near 1/8 doping in cuprates [38,39]. Figure 1 shows the charge density profiles of a ladder with length 192, defined as the rung density $n(x_i) = \sum_{y=1}^{L_y} \langle \hat{n}_i(x, y) \rangle / L_y$ on the ladders. The charge density results from DMRG with numbers of kept states $m = 7000$ to $m = 8500$ and the results from an extrapolation with truncation error are all on top of each other, indicating that the DMRG results are well converged. For the 1/8 hole doping case in Fig. 1, the charge distribution $n(x)$ forms a CDW pattern with a wavelength $\lambda_c = 1/\delta = 8$. The spatial decay of the CDW correlation at long distances can be described by a power law with Luttinger exponent

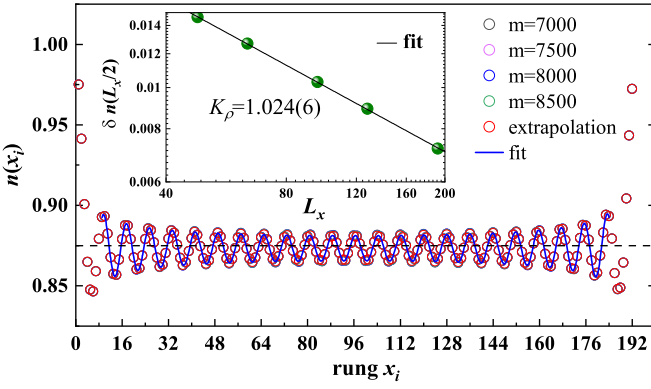


FIG. 1. Density profile at $1/8$ doping. The local rung density $n(x)$ for different numbers of kept states m and the results from extrapolation with truncation errors are shown. The length of the system is $L_x = 192$. The solid curve is the fitting curve using Eq. (2) to extract K_ρ . The dashed horizontal line represents the averaged electron density. The inset shows the finite-size scaling of $\delta n(L_x/2)$ as a function of the system size L_x using Eq. (3).

K_ρ . Previous works [29,33] show that K_ρ can be obtained by fitting the Friedel oscillations induced by the boundaries of the ladder

$$n(x) \approx A \frac{\cos(2\pi N_h x/L_x + \phi_1)}{[L_x \sin(\pi x/L_x + \phi_2)]^{K_\rho/2}} + n_0, \quad (2)$$

where A is the amplitude, ϕ_1 and ϕ_2 are phase shifts, and $n_0 = 1 - \delta$ is the averaged charge density (we set n_0 as a parameter to be determined in the fit [29]). To get rid of the boundary effect, we fit the density by gradually excluding data near the boundaries, and the results are shown in Fig. 2(a) and Table II. We can find an obvious boundary effect on the extracted exponent K_ρ . After excluding about a dozen data points near the boundary, the extracted K_ρ converges fast to a value about 1.02(4), and the R^2 of the fit is very close to 1 (with a deviation of the order of 0.0001). We also study

TABLE II. The dependence of the extracted parameters K_ρ and n_0 [using Eq. (2)] on the range of sites used ($\delta = 1/8$, $L_x = 192$). See also the plot of K_ρ vs the range of sites used in Fig. 2(a).

Range	K_ρ	n_0	R^2
Site 1 to site L_x	1.177(5)	0.8733	0.99692
Site 9 to site $(L_x - 8)$	1.01(1)	0.8734	0.99849
Site 17 to site $(L_x - 16)$	1.01(1)	0.8734	0.99907
Site 25 to site $(L_x - 24)$	1.01(2)	0.8734	0.99931
Site 33 to site $(L_x - 32)$	1.01(2)	0.8734	0.99942
Site 41 to site $(L_x - 40)$	1.01(3)	0.8734	0.99961
Site 49 to site $(L_x - 48)$	1.01(3)	0.8734	0.99981
Site 57 to site $(L_x - 56)$	1.01(3)	0.8734	0.99991
Site 65 to site $(L_x - 64)$	1.03(3)	0.8734	0.99997
Site 73 to site $(L_x - 72)$	1.02(4)	0.8734	0.99999
Site 81 to site $(L_x - 80)$	1.04(8)	0.8734	1

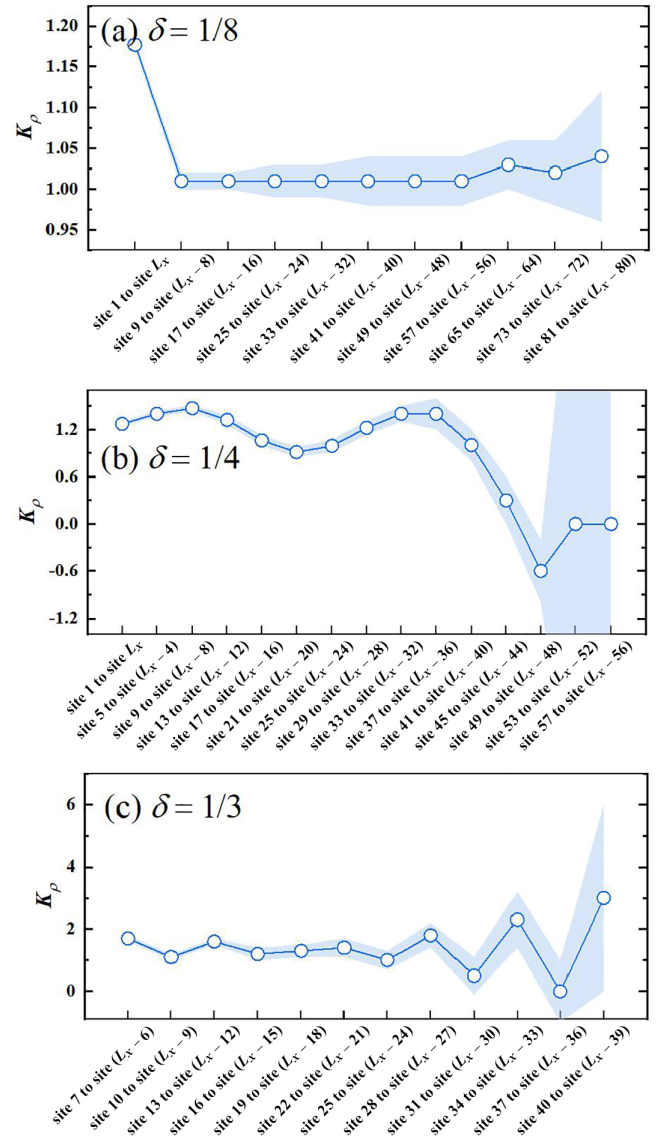


FIG. 2. The dependence of the extracted parameters K_ρ [using Eq. (2)] on the range of sites used for (a) $\delta = 1/8$ ($L_x = 192$), (b) $\delta = 1/4$ ($L_x = 128$), and (c) $\delta = 1/3$ ($L_x = 96$). The shaded region around the curve shows the error bars. The fitted values of K_ρ , n_0 , and R_2 are also listed in Tables II–IV.

ladders with lengths 48, 64, 96, and 128 and find that the extracted values of K_ρ converge. For comparison, we can alternatively obtain the parameter K_ρ from the finite-size scaling, because the density at the center of the system scales as [29]

$$\delta n(L_x/2) = n(L_x/2) - n_0 \sim L_x^{-K_\rho/2}. \quad (3)$$

The advantage of this scheme is that $n(L_x/2)$ is least affected by the boundary effect. The finite-size fit is shown in the inset of Fig. 1. To calculate $\delta n(L_x/2)$, we use the obtained n_0 from the least-squares fit of the charge density profiles using Eq. (2) [29]. Considering the values from the two fitting procedures, we give an estimation of K_ρ at $1/8$ as $K_\rho \approx 1.02(4)$. The values of K_ρ for other dopings are estimated in the same way.

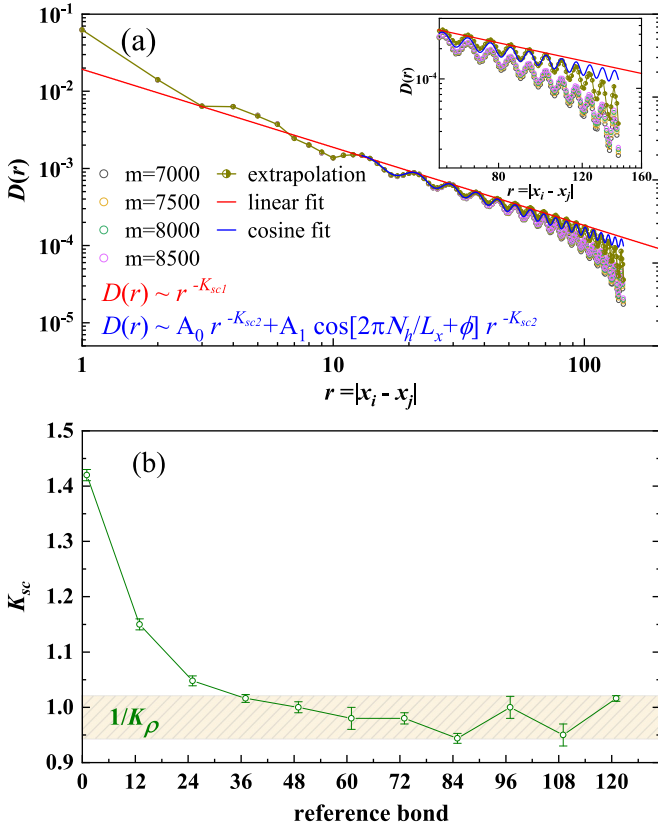


FIG. 3. Pair-pair correlation and the extracted exponents at $1/8$ doping. (a) Pair-pair correlation function $D(r)$ for different numbers of kept states m and the extrapolated result. The length of the system is $L_x = 192$. The reference bond is set at the 49th vertical bond. The red line and blue curve denote the linear and cosine fits, respectively, defined in the main text. Only peaked values are used in the linear fit. The inset zooms in the data scale. (b) K_{sc} as a function of the reference bond. Here we only show the results of K_{sc1} from linear fits (K_{sc2} has similar values). The shaded area represents the value of $1/K_\rho$ with error bars.

The singlet pair-pair correlation function $D(r)$ for the $L_x = 192$ ladder is displayed in Fig. 3. The numerical results are carefully extrapolated with truncation errors in DMRG calculations to remove the finite-bond-dimension effect. We find that $D(r)$ decays algebraically with oscillations in the period of CDW's wavelength λ_c , which makes the extraction of the exponent K_{sc} hard. Apart from fitting the peaks using $D(r) \propto r^{-K_{sc1}}$ as has been typically done before [29,30], we also fit the whole data set by including an extra cosine term as $D(r) \propto A_0 r^{-K_{sc2}} + A_1 \cos(2\pi N_h/L_x + \phi) r^{-K_{sc2}}$, which can be viewed as a first-order approximation to the oscillating pair-pair correlation function. We have checked that both fits give consistent results within the error bars. We also checked that the extracted value of K_{sc} is converged with the size studied.

As can be seen from Fig. 3(a), the pair-pair correlations clearly deviate from the algebraic decay behavior at long distance near the boundary even after an extrapolation with truncation error. So to account for this effect, we exclude the very-long-distance data for all the fits of pair-pair correlations. At the same time, we study long ladders which provide enough data for the fit process.

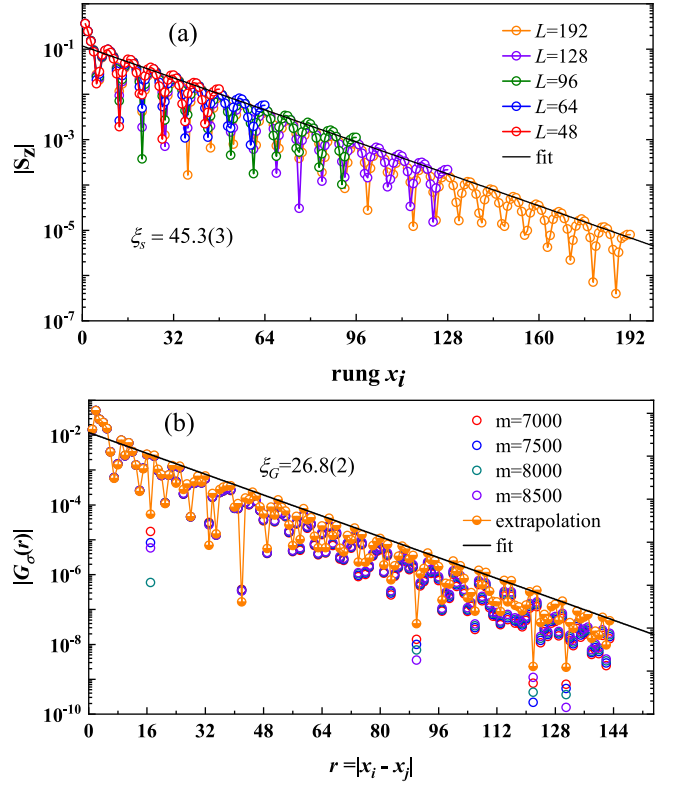


FIG. 4. Local magnetization and single-particle Green's function at $1/8$ doping. (a) Absolute values of the local magnetization with different lengths. We only show the local magnetization on one leg. S_z on different legs are identical in absolute value but with opposite sign. This is also true for other plots of S_z . Only the results from the extrapolation with truncation errors are shown. The solid line denotes the exponential fit using $|S_z| \propto e^{-x_i/\xi_s}$ with $\xi_s = 45.3(3)$ for $L_x = 192$. (b) Single-particle Green's function with different numbers of kept states m and the extrapolated result for $L_x = 192$. The reference site is set at $(49, 2)$. Only peaked values are used in the fits for both the local magnetization and the single-particle Green's function.

In the calculation of the pair-pair correlations, a more important factor is the choice of the position of the reference bond. Figure 3(b) shows the extracted K_{sc} for different reference bonds (only correlations between vertical bonds are shown; the horizontal bonds have similar results). We find that the boundary has a very large effect on K_{sc} . When moving the reference bond away from the boundary, K_{sc} converges, and the converged value satisfies the relationship $K_{sc} \cdot K_\rho = 1$ as predicted in Luther-Emery liquid theory.

Figure 4(a) shows the absolute value of local magnetization for systems with different lengths. We find that $|S_z|$ decays exponentially as $|S_z| \propto e^{-x_i/\xi_s}$ at long distances with a finite correlation length $\xi_s = 45.3(3)$, indicating the existence of a finite spin gap in the system, which is consistent with the prediction of the Luther-Emery liquid phase. Moreover, the staggered spin density $(-1)^{x_i} \langle \hat{S}_i^z \rangle$ (not shown) has a spatial modulation with a wavelength twice that of the hole density and shows a π phase flip at the hole concentrated position.

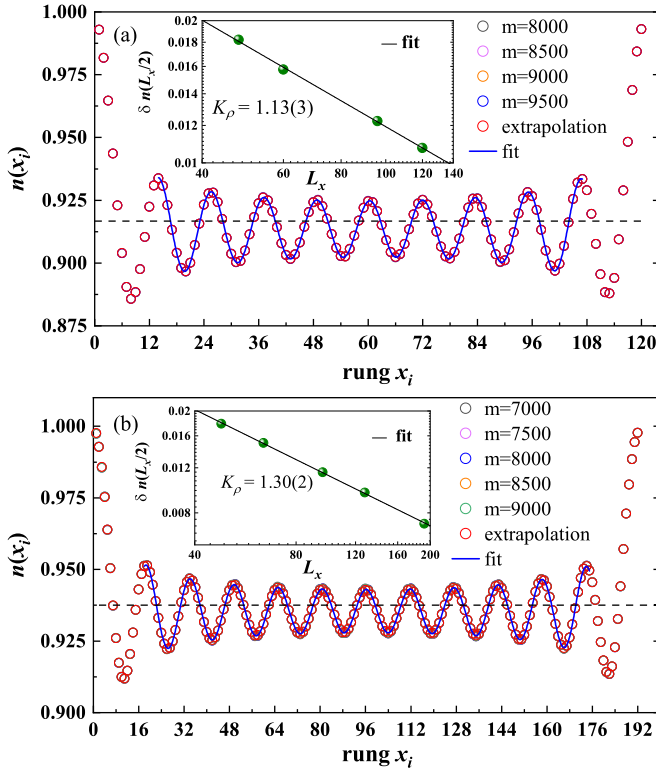


FIG. 5. Density profiles at (a) 1/12 and (b) 1/16 dopings. The local rung density $n(x)$ for different numbers of kept states m and the results from extrapolation with truncation errors are shown. The lengths of the systems are $L_x = 120$ for 1/12 doping and $L_x = 192$ for 1/16 doping. The solid curves are the fitting curves using Eq. (2) to extract K_ρ . The dashed horizontal lines represent the averaged electron density. The insets of (a) and (b) show the finite-size scaling of $\delta n(L_x/2)$ as a function of the system size L_x using Eq. (3).

The spin and hole modulations are consistent with the stripe phase [38,39].

The single-particle Green's function is defined as $G_\sigma(r) = \langle \hat{c}_{(x_0,y),\sigma}^\dagger \hat{c}_{(x_0+r,y),\sigma} \rangle$ with σ being the spin index. We find that $G_\sigma(r)$ is also sensitive to the position of the reference bond, similar to the pair-pair correlations. We only show the converged results in this paper. The results for 1/8 doping are shown in Fig. 4(b). $G_\sigma(r)$ decays exponentially as $|G_\sigma(r)| \propto e^{-r/\xi_G}$ with the correlation length $\xi_G = 26.8(2)$.

From the above analysis of the charge, pairing correlation, local magnetization, and single-particle Green's function, we conclude that the two-legged ladder at 1/8 doping with $U = 8$ belongs to the Luther-Emery liquid phase and the exponents of the charge and superconducting correlations satisfy the relationship $K_{sc} \cdot K_\rho = 1$.

B. 1/12 and 1/16 dopings

We perform similar calculations and analyses for 1/12 and 1/16 dopings in this section. The charge density profiles for 1/12 and 1/16 dopings are shown in Figs. 5(a) and 5(b), which also display the Friedel oscillations with $\lambda_c = 1/\delta$. We find that the amplitude of charge density oscillations is reduced with the decrease in the doping level. The exponent increases from $K_\rho = 1.13(3)$ to $K_\rho = 1.28(3)$ from $\delta = 1/12$

TABLE III. The dependence of the extracted parameters K_ρ and n_0 [using Eq. (2)] on the range of sites used ($\delta = 1/4$, $L_x = 128$). See also the plot of K_ρ vs the range of sites used in Fig. 2(b).

Range	K_ρ	n_0	R^2
Site 1 to site L_x	1.27(3)	0.7495	0.97288
Site 5 to site (L_x-4)	1.40(4)	0.7494	0.97634
Site 9 to site (L_x-8)	1.47(4)	0.7495	0.98724
Site 13 to site (L_x-12)	1.32(6)	0.7495	0.98481
Site 17 to site (L_x-16)	1.06(7)	0.7495	0.99076
Site 21 to site (L_x-20)	0.91(6)	0.7494	0.99565
Site 25 to site (L_x-24)	0.99(8)	0.7494	0.99638
Site 29 to site (L_x-28)	1.22(9)	0.7494	0.99720
Site 33 to site (L_x-32)	1.4(1)	0.7494	0.99807
Site 37 to site (L_x-36)	1.4(2)	0.7494	0.99794
Site 41 to site (L_x-40)	1.0(2)	0.7494	0.99802
Site 45 to site (L_x-44)	0.3(3)	0.7494	0.99879
Site 49 to site (L_x-48)	-0.6(4)	0.7494	0.99921
Site 53 to site (L_x-52)	0(4)	0.7494	0.99899
Site 57 to site (L_x-56)	0(19)	0.7494	0.99916

to $\delta = 1/16$ (see the insets of Fig. 5 and Table I). This behavior is consistent with the prediction that $K_\rho \rightarrow 2$ with $\delta \rightarrow 0$ [34,35].

Following the fitting procedures in the 1/8 doping case, we also extract K_{sc} from the pair-pair correlations by varying the position of the reference bond as shown in Figs. 6(a) and 6(d). The converged values for K_{sc} are 0.95(3) and 0.85(5) for 1/12 and 1/16 dopings, respectively. For these dopings, $K_{sc} < K_\rho$, indicating that the superconducting correlation is dominant at low dopings [29]. Similarly to the 1/8 doping case, the relationship $K_{sc} \cdot K_\rho = 1$ is also likely to be satisfied, which is consistent with the prediction from Luther-Emery liquid theory.

The absolute value of the local magnetization and the single-particle Green's function for 1/12 (1/16) doping are shown in Figs. 6(b) and 6(c) [Figs. 6(e) and 6(f)], respectively. Both of them decay exponentially with distance, and the correlation lengths are smaller than 1/8 cases, indicating that the spin and single-particle gap increase with the decrease in doping.

C. 1/6 doping level

In this section, we move to the 1/6 doping case. Figure 7 shows the charge density profiles for a $L_x = 120$ ladder, which is also characterized by an algebraic quasi-long-range order with period $\lambda_c = 1/\delta = 6$. As we can see in the inset of Fig. 7, the K_ρ values extracted from the two approaches are consistent with $K_\rho \approx 1.01(4)$. Following the procedure described above, we show the variance of K_{sc} with the position of the reference bond in Fig. 8(a). We find that $K_\rho < K_{sc}$ (see also

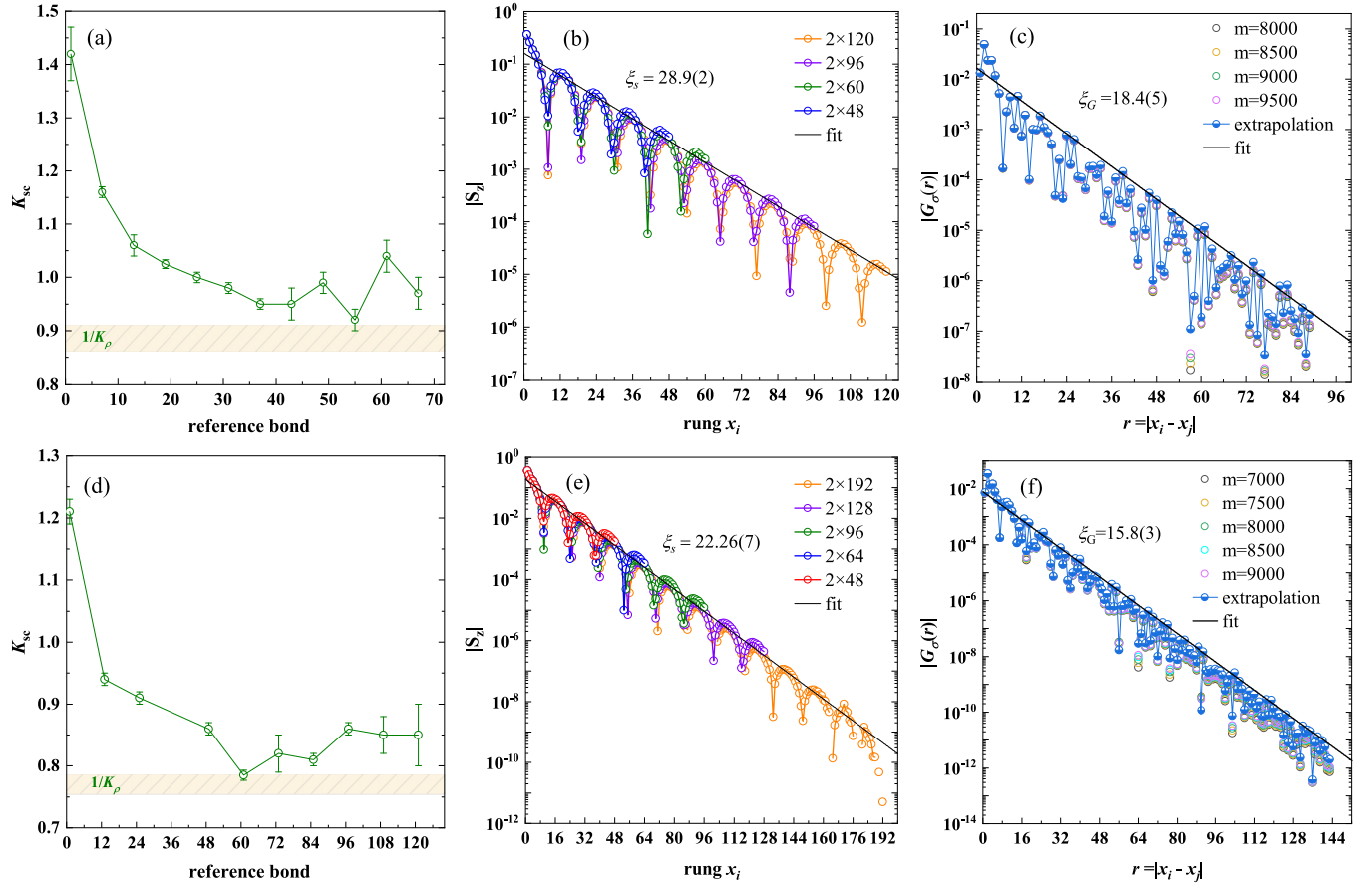


FIG. 6. Results for 1/12 [(a)–(c)] and 1/16 [(d)–(f)] dopings. (a) and (d) show K_{sc} as a function of the reference bond. The lengths of the systems are $L_x = 120$ for $\delta = 1/12$ and $L_x = 192$ for $\delta = 1/16$. The shaded area represents the value of $1/K_\rho$ with error bars. (b) and (e) show the absolute values of the local magnetization at 1/12 and 1/16 dopings with different lengths. Only the results from the extrapolation with truncation errors are shown. The solid lines denote exponential fits using $|S_i| \propto e^{-x_i/\xi_s}$ with $\xi_s = 28.9(2)$ for $\delta = 1/12$ ($L_x = 120$) and $\xi_s = 22.26(7)$ for $\delta = 1/16$ ($L_x = 192$). (c) and (f) show the single-particle Green's function for different numbers of kept states m and the extrapolated result. The reference site is set at (31, 2) for $\delta = 1/12$ ($L_x = 120$) and (49, 2) for $\delta = 1/16$ ($L_x = 192$). Only peaked values are used in the fits for both the local magnetization and the single-particle Green's function.

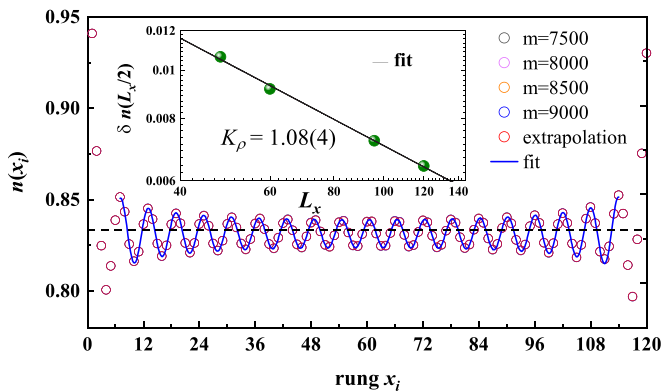


FIG. 7. Density profile at 1/6 doping. The local rung density $n(x)$ for different numbers of kept states m and the results from extrapolation with truncation error are shown. The length of the system is $L_x = 120$ at 1/6 doping. The solid curve is the fitting curve using Eq. (2) to extract K_ρ . The dashed horizontal line represents the average electron density. The inset shows the finite-size scaling of $\delta n(L_x/2)$ as a function of the system size L_x using Eq. (3).

Table I), suggesting that the charge correlation is dominating at 1/6 doping. We find that charge and superconducting exponents are likely to violate the relationship $K_{sc} \cdot K_\rho = 1$. The local magnetization and single-particle Green's function are shown in Figs. 8(b) and 8(c). Both of them decay exponentially with correlation lengths $\xi_s = 67.6(2)$ and $\xi_G = 36(2)$.

D. 1/3 and 1/4 dopings

Figure 9(a) shows the charge density profile at 1/4 doping for a $L_x = 128$ ladder. We can see that the charge modulation has a persistent amplitude with period $\lambda_c = 1/\delta$ which does not decay in the bulk. The extracted K_ρ values using Eq. (2) are shown in Fig. 2(b) and Table III. The value of K_ρ varies dramatically with the data range used in the fit. The fact that K_ρ has very large error bars and oscillates across zero indicates the failure of the fit using Eq. (2), which suggests that the charge order is likely long ranged in the system.

The pair-pair correlations for $\delta = 1/4$ are shown in Figs. 10(a) and 10(b). Following the same procedure above, we find $K_{sc} = 1.05(6)$ at $\delta = 1/4$. We show the local magnetization on both semilogarithmic and double-logarithmic

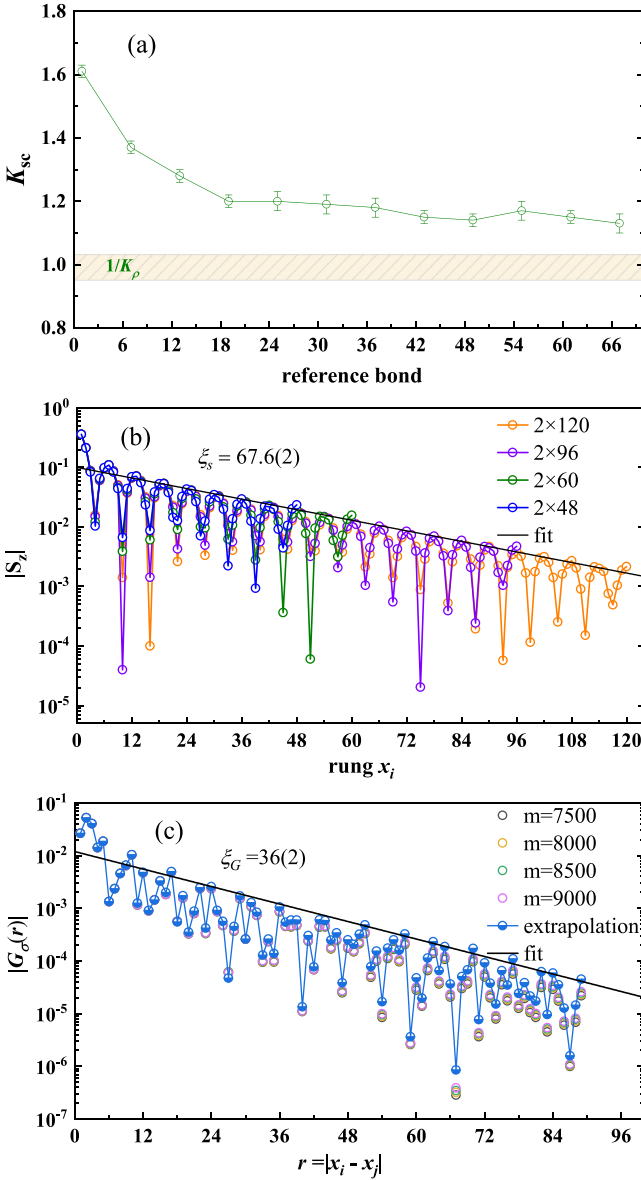


FIG. 8. Results for the 1/6 doping level. (a) shows K_{sc} as a function of the reference bond. The length of the system is $L_x = 120$. The shaded area represents the value of $1/K_\rho$ with error bars. (b) shows the absolute value of the local magnetization at 1/6 doping for systems with different lengths. Only the results from the extrapolation with truncation errors are shown. The solid line denotes exponential fitting using $|S_z| \propto e^{-x_i/\xi_s}$ with $\xi_s = 67.6(2)$ for $L_x = 120$. (c) shows the single-particle Green's function for different numbers of kept states m and the extrapolated result. The reference site is set at (31, 2). Only peaked values are used in the exponential fits for both the local magnetization and the single-particle Green's function.

scales in Figs. 10(c) and 10(d). We find that the data are better described by an exponential decay fit with a very large correlation length $\xi_s = 107(2)$ instead of a power-law decay. The single-particle Green's function is found to decay exponentially with a correlation length $\xi_G = 50(2)$ [see Figs. 10(e) and 10(f)].

The results for 1/3 doping are similar to those for 1/4 doping. The charge order is likely to be a long-ranged one as

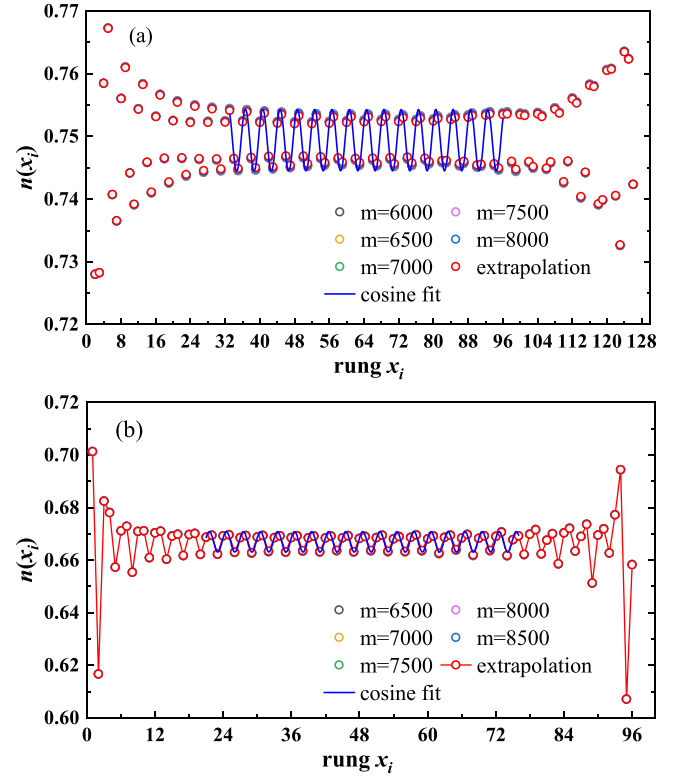


FIG. 9. Density profiles at (a) 1/4 and (b) 1/3 dopings. The local rung density $n(x)$ for different numbers of kept states m and the results from extrapolation with truncation errors are shown. The lengths of the systems are $L_x = 128$ for 1/4 doping and $L_x = 96$ for 1/3 doping. The solid curves are the fitting curves using a cosine function.

TABLE IV. The dependence of the extracted parameters K_ρ and n_0 [using Eq. (2) on the range of sites used ($\delta = 1/3$, $L_x = 96$)]. See also the plot of K_ρ vs the range of sites used in Fig. 2(c).

Range	K_ρ	n_0	R^2
Site 7 to site ($L_x - 6$)	1.7(1)	0.6670	0.94290
Site 10 to site ($L_x - 9$)	1.1(1)	0.6670	0.95782
Site 13 to site ($L_x - 12$)	1.6(1)	0.6670	0.97182
Site 16 to site ($L_x - 15$)	1.2(2)	0.6670	0.97694
Site 19 to site ($L_x - 18$)	1.3(2)	0.6670	0.98024
Site 22 to site ($L_x - 21$)	1.4(3)	0.6670	0.98320
Site 25 to site ($L_x - 24$)	1.0(3)	0.6670	0.98523
Site 28 to site ($L_x - 27$)	1.8(4)	0.6670	0.98850
Site 31 to site ($L_x - 30$)	0.5(6)	0.6670	0.99027
Site 34 to site ($L_x - 33$)	2.3(9)	0.6670	0.99246
Site 37 to site ($L_x - 36$)	0(1)	0.6670	0.99308
Site 40 to site ($L_x - 39$)	3(3)	0.6670	0.99320

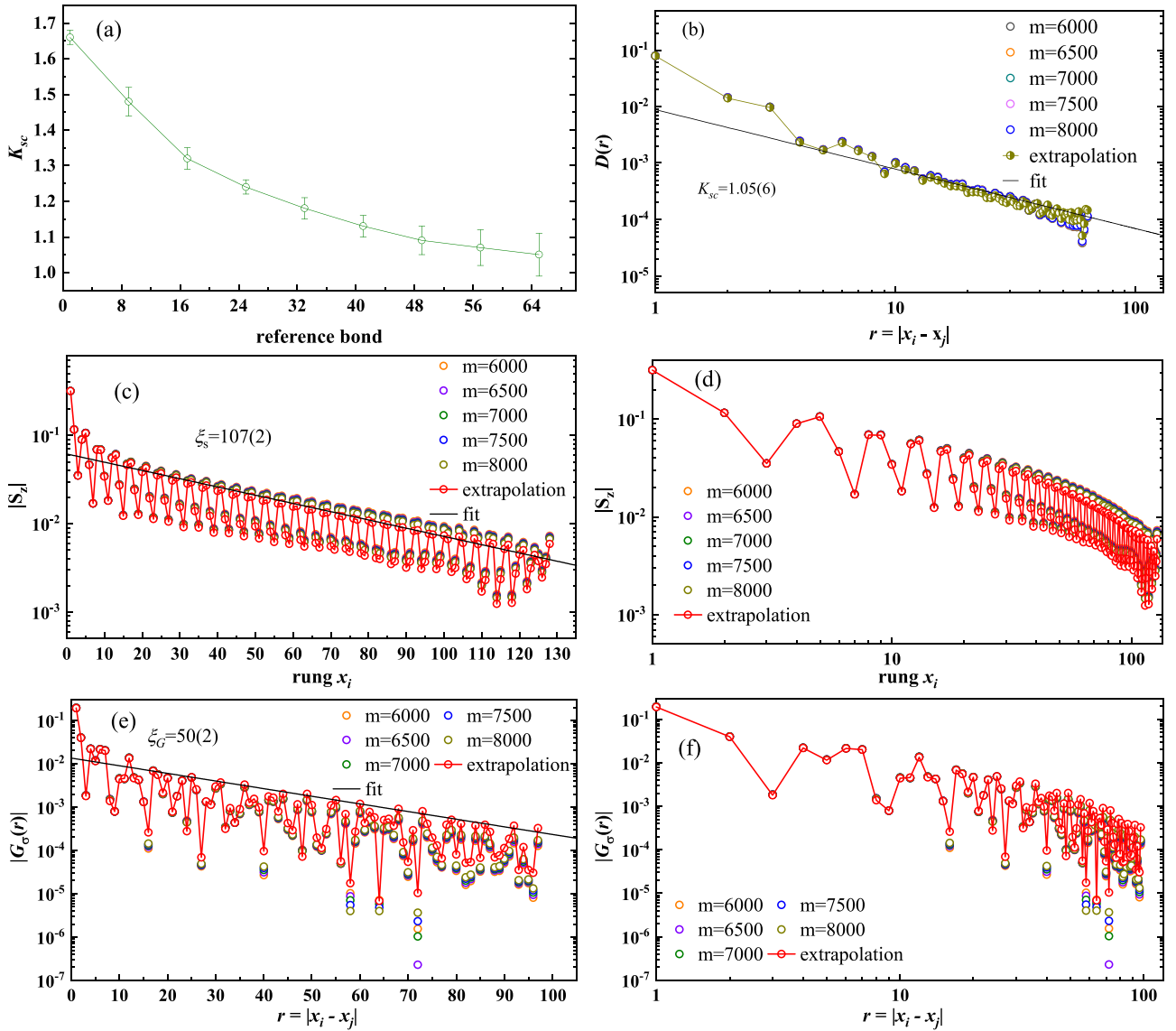


FIG. 10. Pair-pair correlation, local magnetization, and the single-particle Green's function at 1/4 doping. (a) K_{sc} as a function of the reference bond. The length of the system is $L_x = 128$. (b) A typical fit of the pair-pair correlation function. The reference bond is set at the 65th vertical bond. (c) and (d) Absolute value of local magnetization and (e) and (f) single-particle Green's function. The results from finite numbers of kept states and the results from extrapolation with truncation errors are shown. The plots in (c) and (e) and those in (d) and (f) have semilogarithmic and double-logarithmic axes, respectively. The solid black line in (c) denotes exponential fitting using $|S_z| \propto e^{-x_i/\xi_s}$ with $\xi_s = 107(2)$. By comparing (c) and (d), we find that the decay of the local magnetization is likely to be exponential, even though the extracted correlation length is comparable to the length of the system. The single-particle Green's function is also more likely to exhibit exponential decay. Only peaked values are used in the fits.

shown in Fig. 9(b). In Fig. 2(c) and Table IV, we find that the extracted value of K_ρ also varies dramatically with the data range. The extracted $K_{sc} = 1.10(8)$ as shown in Figs. 11(a) and 11(b). The spatial decay of local magnetization can be well fitted using either an exponential law or a power law but with correlation length equal to the size of the system [see Figs. 11(c) and 11(d)], indicating that the spin gap is likely to be closed at 1/3 doping. The decay of single-particle Green's function is found to be power-law-like, indicating the closing of the gap at 1/3 doping [see Figs. 11(e) and 11(f)].

IV. CONCLUSIONS

We revisit the ground state of the Hubbard model on two-legged ladders with DMRG. We find that K_{sc} extracted from the algebraic decay of the pair-pair correlation depends strongly on the position of the reference bond. We obtain more accurate exponents K_ρ and K_{sc} with DMRG after systematically treating the effects from boundary conditions, finite sizes, and truncation errors in DMRG. We confirm that the two-legged Hubbard model is in the Luther-Emery liquid phase with $K_\rho \cdot K_{sc} = 1$ from tiny doping near half filling to

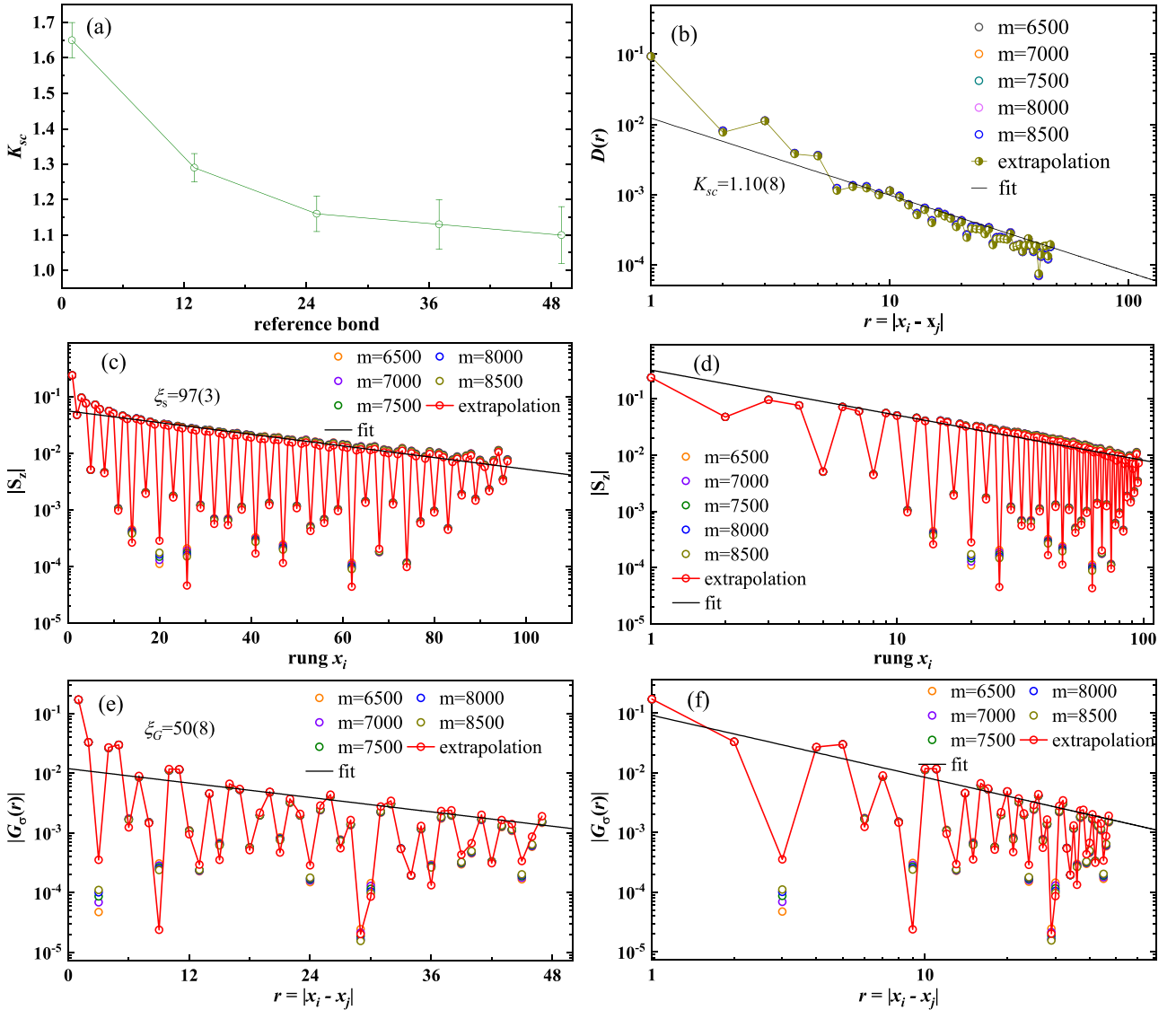


FIG. 11. Pair-pair correlation, local magnetization, and the single-particle Green's function at $1/3$ doping. (a) K_{sc} as a function of the reference bond. The length of the system is $L_x = 96$. (b) A typical fit of the pair-pair correlation function. The reference bond is set at the 49th vertical bond. (c) and (d) Absolute value of the spin density and (e) and (f) single-particle Green's function. The results from finite numbers of kept states and the results from extrapolation with truncation errors are shown. The solid black lines in (c) and (e) and those in (d) and (f) denote exponential and power-law fits, respectively. For spin density, we find that the data can be fitted with either an exponential fit or a power-law fit. However, the correlation length extracted from the power-law fit is larger than the system size, which indicates that the decay of the local magnetization is likely to be a power law. For single-particle excitation, we also find that the decay behavior of $G_\sigma(r)$ can be fitted with either an exponential fit or a power-law fit. Only peaked values are used in the fits.

$1/8$ hole doping, resolving the long-term controversy. When the doping is increased to $\delta \gtrsim 1/6$, the behaviors of charge, pairing, and spin correlations do not change qualitatively, but the relationship $K_{sc} \cdot K_\rho = 1$ is likely to be violated. With the further increase of the doping to $\delta = 1/3$, the quasi-long-ranged charge correlation turns into a long-ranged charge order, and the spin gap is closed, while the pair-pair correlation still decays algebraically. In Ref. [37], the Hubbard ladder at $1/3$ doping with next-nearest-neighbor hopping t' and a larger $U = 12$ was studied [37]. The charge correlation was found to decay algebraically, while the spin and single-particle excitations are gapped [37]. A comparison of the results in Ref. [37] and in this paper indicates that the boundary of

different phases depends on the details of the parameters in the model. Our work provides a standard way to analyze the correlation functions when studying systems with open boundaries.

ACKNOWLEDGMENTS

We thank Xingjie Han for useful discussions. Y.S. and M.Q. thank Weidong Luo for generosity in providing the computational resources for this work. M.Q. acknowledges support from the National Key Research and Development Program of MOST of China (Grant No. 2022YFA1405400),

the National Natural Science Foundation of China (Grant No. 12274290), the Innovation Program for Quantum Science and Technology (Grant No. 2021ZD0301900), and

the sponsorship from Yangyang Development Fund. All the DMRG calculations were carried out with the ITENSOR library [40].

-
- [1] J. Hubbard, *Proc. R. Soc. London A* **276**, 238 (1963).
- [2] D. P. Arovas, E. Berg, S. A. Kivelson, and S. Raghu, *Annu. Rev. Condens. Matter Phys.* **13**, 239 (2022).
- [3] M. Qin, T. Schäfer, S. Andergassen, P. Corboz, and E. Gull, *Annu. Rev. Condens. Matter Phys.* **13**, 275 (2022).
- [4] E. Dagotto, *Rev. Mod. Phys.* **66**, 763 (1994).
- [5] A. Himeda, T. Kato, and M. Ogata, *Phys. Rev. Lett.* **88**, 117001 (2002).
- [6] E. Gull, O. Parcollet, and A. J. Millis, *Phys. Rev. Lett.* **110**, 216405 (2013).
- [7] A. S. Darmawan, Y. Nomura, Y. Yamaji, and M. Imada, *Phys. Rev. B* **98**, 205132 (2018).
- [8] B. Ponsioen, S. S. Chung, and P. Corboz, *Phys. Rev. B* **100**, 195141 (2019).
- [9] M. Qin, C.-M. Chung, H. Shi, E. Vitali, C. Hubig, U. Schollwöck, S. R. White, and S. Zhang (Simons Collaboration on the Many-Electron Problem), *Phys. Rev. X* **10**, 031016 (2020).
- [10] C.-M. Chung, M. Qin, S. Zhang, U. Schollwöck, and S. R. White (The Simons Collaboration on the Many-Electron Problem), *Phys. Rev. B* **102**, 041106(R) (2020).
- [11] S. Jiang, D. J. Scalapino, and S. R. White, *Proc. Natl. Acad. Sci. USA* **118**, e2109978118 (2021).
- [12] S. Gong, W. Zhu, and D. N. Sheng, *Phys. Rev. Lett.* **127**, 097003 (2021).
- [13] H.-C. Jiang and S. A. Kivelson, *Phys. Rev. Lett.* **127**, 097002 (2021).
- [14] H. Xu, C.-M. Chung, M. Qin, U. Schollwöck, S. R. White, and S. Zhang, [arXiv:2303.08376](https://arxiv.org/abs/2303.08376).
- [15] J. G. Bednorz and K. A. Müller, *Z. Phys. B* **64**, 189 (1986).
- [16] E. H. Lieb and F. Y. Wu, *Phys. Rev. Lett.* **20**, 1445 (1968).
- [17] J. P. F. LeBlanc, A. E. Antipov, F. Becca, I. W. Bulik, G. K.-L. Chan, C.-M. Chung, Y. Deng, M. Ferrero, T. M. Henderson, C. A. Jiménez-Hoyos, E. Kozik, X.-W. Liu, A. J. Millis, N. V. Prokof'ev, M. Qin, G. E. Scuseria, H. Shi, B. V. Svistunov, L. F. Tocchio, I. S. Tupitsyn *et al.* (Simons Collaboration on the Many-Electron Problem), *Phys. Rev. X* **5**, 041041 (2015).
- [18] M. Troyer, H. Tsunetsugu, and T. M. Rice, *Phys. Rev. B* **53**, 251 (1996).
- [19] L. Balents and M. P. A. Fisher, *Phys. Rev. B* **53**, 12133 (1996).
- [20] U. Schollwöck, *Rev. Mod. Phys.* **77**, 259 (2005).
- [21] C. Wu, W. Vincent Liu, and E. Fradkin, *Phys. Rev. B* **68**, 115104 (2003).
- [22] Y. He, D. M. Kennes, C. Karrasch, and R. Rausch, [arXiv:2302.14085](https://arxiv.org/abs/2302.14085).
- [23] Z. Zhou, W. Ye, H.-G. Luo, J. Zhao, and J. Chang, [arXiv:2303.14723](https://arxiv.org/abs/2303.14723).
- [24] S. R. White, *Phys. Rev. Lett.* **69**, 2863 (1992).
- [25] S. R. White, *Phys. Rev. B* **48**, 10345 (1993).
- [26] U. Schollwöck, *Ann. Phys. (Amsterdam)* **326**, 96 (2011).
- [27] A. Luther and V. J. Emery, *Phys. Rev. Lett.* **33**, 589 (1974).
- [28] F. D. M. Haldane, *Phys. Rev. Lett.* **45**, 1358 (1980).
- [29] M. Dolfi, B. Bauer, S. Keller, and M. Troyer, *Phys. Rev. B* **92**, 195139 (2015).
- [30] X. Lu, D.-W. Qu, Y. Qi, W. Li, and S.-S. Gong, *Phys. Rev. B* **107**, 125114 (2023).
- [31] R. M. Noack, N. Bulut, D. J. Scalapino, and M. G. Zacher, *Phys. Rev. B* **56**, 7162 (1997).
- [32] R. Noack, S. White, and D. Scalapino, *Phys. C (Amsterdam)* **270**, 281 (1996).
- [33] S. R. White, I. Affleck, and D. J. Scalapino, *Phys. Rev. B* **65**, 165122 (2002).
- [34] H. J. Schulz, *Phys. Rev. B* **59**, R2471(R) (1999).
- [35] T. Siller, M. Troyer, T. M. Rice, and S. R. White, *Phys. Rev. B* **63**, 195106 (2001).
- [36] A. A. Eberharter, L. Vanderstraeten, F. Verstraete, and A. M. Läuchli, [arXiv:2303.00663](https://arxiv.org/abs/2303.00663).
- [37] Y. Shen, M. Qin, and G.-M. Zhang, *Phys. Rev. B* **107**, 165103 (2023).
- [38] J. Tranquada, B. Sternlieb, J. Axe, Y. Nakamura, and S.-i. Uchida, *Nature (London)* **375**, 561 (1995).
- [39] V. J. Emery, S. A. Kivelson, and J. M. Tranquada, *Proc. Natl. Acad. Sci. USA* **96**, 8814 (1999).
- [40] M. Fishman, S. R. White, and E. M. Stoudenmire, *SciPost Phys. Codebases*, 4 (2022).